nature photonics

SUPPLEMENTARY INFORMATION

https://doi.org/10.1038/s41566-019-0509-0

In the format provided by the authors and unedited.

Quantum wave–particle superposition in a delayed-choice experiment

Kai Wang, Qian Xu, Shining Zhu and Xiao-song Ma*

National Laboratory of Solid State Microstructures, School of Physics and Collaborative Innovation Center of Advanced Microstructures, Nanjing University, Nanjing, China. *e-mail: Xiaosong.Ma@nju.edu.cn

Supplementary Information: Quantum wave–particle superposition in a delayed-choice experiment

Kai Wang, Qian Xu, Shining Zhu, and Xiao-song Ma*
National Laboratory of Solid-state Microstructures & School of Physics,
Collaborative Innovation Center of Advanced Microstructures, Nanjing University, China
(Dated: August 1, 2019)

I. LAB1: EXPERIMENTAL DETAILS OF THE MACH-ZEHNDER AND HONG-OU-MANDEL INTERFEROMETERS

The goal of our experiment is to realize a Mach-Zehnder interferometer (MZI) with the quantum controlled Hadamard (CH) gate, acting as the output beam splitter (BS2 in Fig.1**c** of the main text). In order to realize this goal, we embed the MZI into a two-photon Hong-Ou-Mandel interferometer (HOMI)[1], which enables us to realize the CH gate based on measurement-induced nonlinearity [2–4]. The schematic of our setup in Lab1 is shown in Fig.1.

We use a polarization Mach-Zehnder Interferometer (MZI), in which the first beam splitter (BS1 in Fig. 1**c** of the main text) is realized with a half-wave plate (HWP1) with its optical axis orienting along 22.5°. Phase φ is adjusted by Soleil-Babinet compensator (SBC). A controlled-Pauli-Z (CZ) gate is made by three partial polarization beam splitters (PPBS1-3) and four half-wave plates (HWP3-6). Two W gates, realized with HWP2 and HWP7 oriented along 11.25°, and the CZ gate constitute a controlled-Hardmard (CH) gate in the following form:

$$\mathbf{CH_{CS}} = (\mathbf{I}_C \otimes \mathbf{W}_S)\mathbf{CZ}_{CS}(\mathbf{I}_C \otimes \mathbf{W}_S), \tag{1}$$

which acts as BS_2 in Fig. 1**c** of the main text, where

$$\text{CH gate} : \mathbf{CH_{CS}} = \begin{bmatrix} 1 & 0 & 0 & 0 \\ 0 & 1 & 0 & 0 \\ 0 & 0 & \frac{1}{\sqrt{2}} & \frac{1}{\sqrt{2}} \\ 0 & 0 & \frac{1}{\sqrt{2}} & -\frac{1}{\sqrt{2}} \end{bmatrix} \tag{2}$$

$$\text{W gate} : \mathbf{W}_{\mathrm{S}} = \begin{bmatrix} \cos\pi/8 & \sin\pi/8 \\ \sin\pi/8 & -\cos\pi/8 \end{bmatrix} \tag{3}$$

$$\text{Controled} - \text{Z gate} : \mathbf{CZ}_{\mathrm{CS}} = \begin{bmatrix} 1 & 0 & 0 & 0 \\ 0 & 1 & 0 & 0 \\ 0 & 0 & 1 & 0 \\ 0 & 0 & 0 & -1 \end{bmatrix} \tag{4}$$

$$\text{Identity gate} : \mathbf{I}_{\mathrm{C}} = \begin{bmatrix} 1 & 0 \\ 0 & 1 \end{bmatrix}. \tag{5}$$

The subscripts represent photons being manipulated.

All the PPBSs we used in the CZ gate have the similar optical specifications with the ratio of horizontal and vertical polarized light's transmission coefficients equalling to $T_H : T_V = 3 : 1$. To facilitate the CZ gate, we have to coherently overlap photons S and C on CZ. This is confirmed by the observations of HOM interference dip, which is realized by scanning the delay of photon S with respect to photon C. SBC introduces various birefringent phases, φ, for photon S as we adjust the thickness of SBC. We measure HOM interference patterns with phase φ changing from 0 to 2π, shown in Fig. 2**a-i**. These results show a relation between the position of HOM dip and phase φ, as in Fig. 2**j**. According to this relation, we set different values of the delay (corresponding to the position of HOM dip) for different phases in our experiment.

* E-mail: Xiaosong.Ma@nju.edu.cn

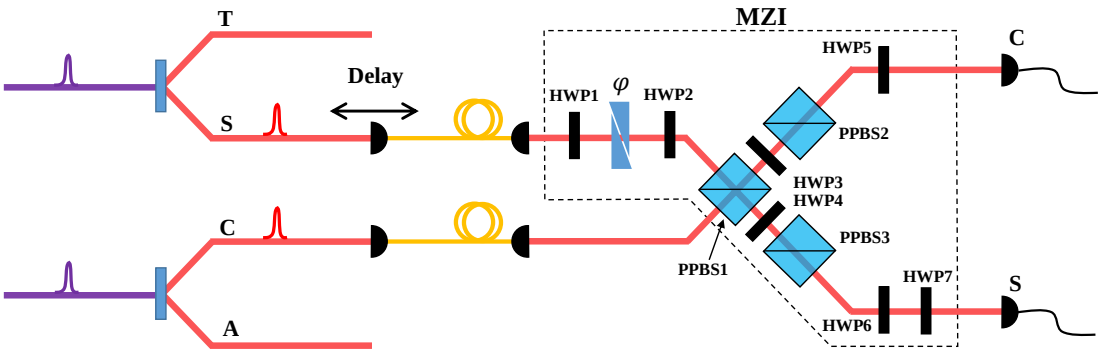

FIG. 1. Simplified experimental setup in Lab1. The Mach-Zehnder Interferometer (MZI) for photon S is realized with several polarization optical elements, as stated in the text. We introduce delay for photon S with respect to photon C using a motorized translation stage which moves along the optical path to scan HOM interference pattern.

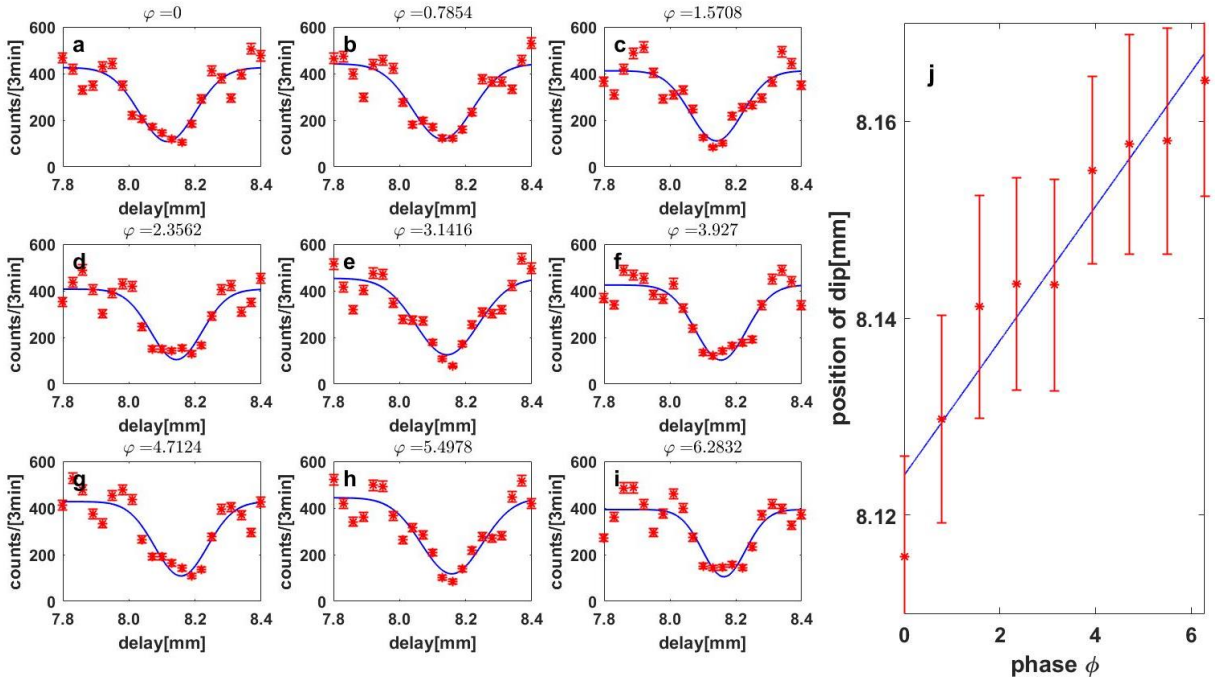

FIG. 2. The relations between phase φ and HOM-dip positions. (**a-i**) The HOM interference patterns have been measured at the different phase φ from about 0 to 2π. Horizontal axis represents the position of the translation stage, which introduces the optical delay. Vertical axis represents the four-fold coincidence count $|HVVH\rangle_{TSCA}$. In ideal condition, HOM interference on PPBS gives a contrast value of 0.8 (C=(Max-Min)/Max). Fitting curves of our experimental data give the average contrast 0.738 ± 0.084. (**j**) Linear fit of the position of HOM dip as a function of phase φ. The error bar represent standard deviation and is obtained from curve fitting. Each point corresponds to one figure in **a-i**.

II. LAB2: EXPERIMENTAL DETAILS OF PHOTON A'S MEASUREMENT SETUP

Our setup of Lab2 is shown in Fig.3. To implement fast optical switch between $|H\rangle/|V\rangle$ and $|\alpha\rangle/|\alpha^{\perp}\rangle$ basis, we use an electro-optic modulator (EOM) with optical axis oriented along 45° relative to the laboratory coordinates and two HWPs at the angle θ. When random number is 1, $\alpha = 0°$; when it is 0, $\alpha = 4\theta - \frac{\pi}{2}$. After the rotation of angle α, photon A is detected in $|H\rangle/|V\rangle$ basis. The details of electric and optical signal processing are shown in Fig. 3**a**. A quantum random number generator (QRNG), driven by 5 MHz square-wave signals from function generator (FG), takes about 80 ns to response to the driving signal and then streams out random numbers as shown in Fig. 3**b**. The random number signals (RNS) are divided into two identical copies, RNS1 and RNS2, respectively. RNS1 signals are

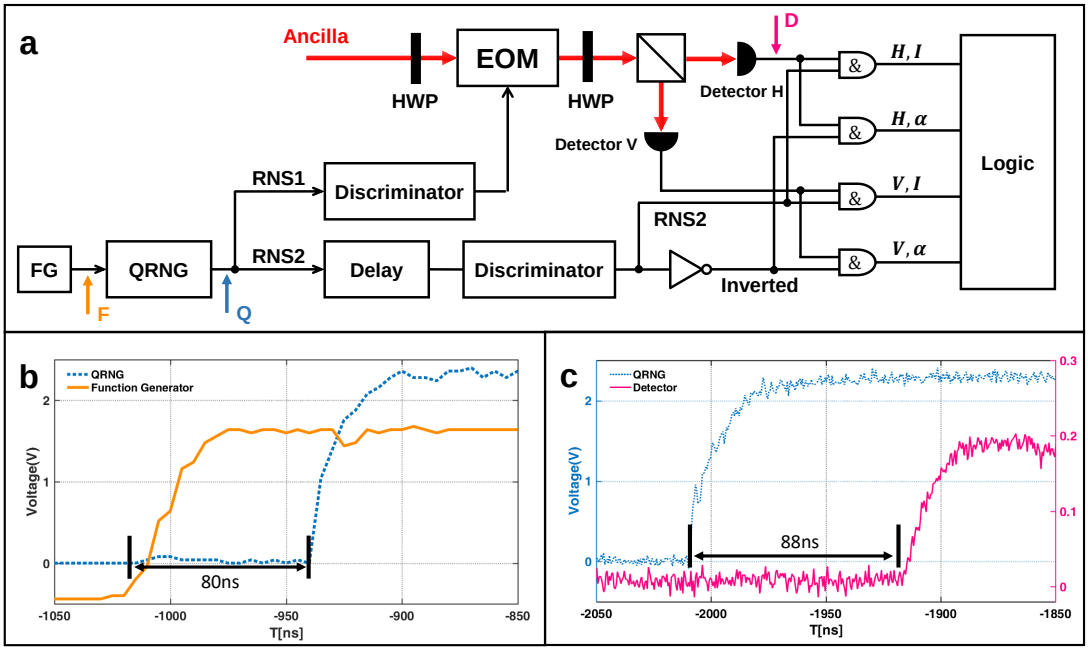

FIG. 3. Setup in Lab2. (**a**) Electric and optical signals processing scheme. A function generator (FG) sends signals to drive QRNG to generate random number number stream at the frequency of 5 MHz. The random number signals are divided into RNS1 and RNS2. RNS1 signals drive the EOM. RNS2 signals categorize the detector signals. Logic circuit analyses and counts the categorized detector signals. Three marked arrows F,Q,D represent the signals from FG,QRNG and Detector H being present at the corresponding locations. Their temporal separations are shown in Fig. 3**b**,**c**. (**b**) Response of QRNG to FG signal. Orange solid/blue dashed curve represents the trigger from the FG/the output random number signals from QRNG at the location of F/Q, respectively. QRNG takes about 80 ns to response the trigger signal. (**c**) Blue dashed and red solid curves respectively represent the random number signals from QRNG and the detection signals from Detector H, showing the modulation effect of EOM. The time interval of these two signals is about 88ns. The whole process from quantum random number input to photon detection output is contained in this period.

shaped with a discriminator, amplified by the EOM driver and sent to EOM. EOM responses to the driving signal and modulates the transmitting light accordingly. Then we use two photon detectors (denoted as Detector H/V for horizontal/vertical polarization) on each output port of the PBS to analyze the polarization of output light. The whole process from quantum random number input to single-photon detection output takes 88 ns as shown in Fig. 3**c**. RNS2 signals are used to make coincidence counts and hence we can categorize the detector signals: photons being modulated at the high or low level of random number signals, corresponding to I/α gate operation. Then RNS2 and inverted RNS2 will both do **AND** operation with signal pulses from detectors and logic circuit counts the resulting four coincidence counts: Detector **H** with Identity(I); Detector **H** with α gate; Detector **V** with Identity; Detector **V** with α gate.

In order to find the exact temporal delay of RNS2 signals for compensating the EOM and detector's response, we sent photons in $|H\rangle$ state into the EOM oriented at 45° (Fig. 4**a**). At the low level of random number signal, EOM will rotate the polarization states of photons to $|V\rangle$ state and Detector V fires; at the high level, the polarization states of photon keep unchanged and only Detector H fires as shown in Fig. 4**c**. The signal pulses from Detector H will do **AND** operation with RNS2 and inverted RNS2 (Fig. 4**e**,**f**) . When we find the right delay between RNS2 and detector pulses, there should be a maximum contrast between the output counts of the two **AND** gate. This is because that, at the high level of random number signals, the polarization states of the photon are mainly at $|H\rangle$. In our experiment, we obtained a maximum contrast about 18:1 with 5 MHz random number signal with the correct delay. This is shown with the single-photon counting results in Fig.5. Complementary illustrations of Detector **V** are shown in Fig. 4**g**, **h** and **i**.

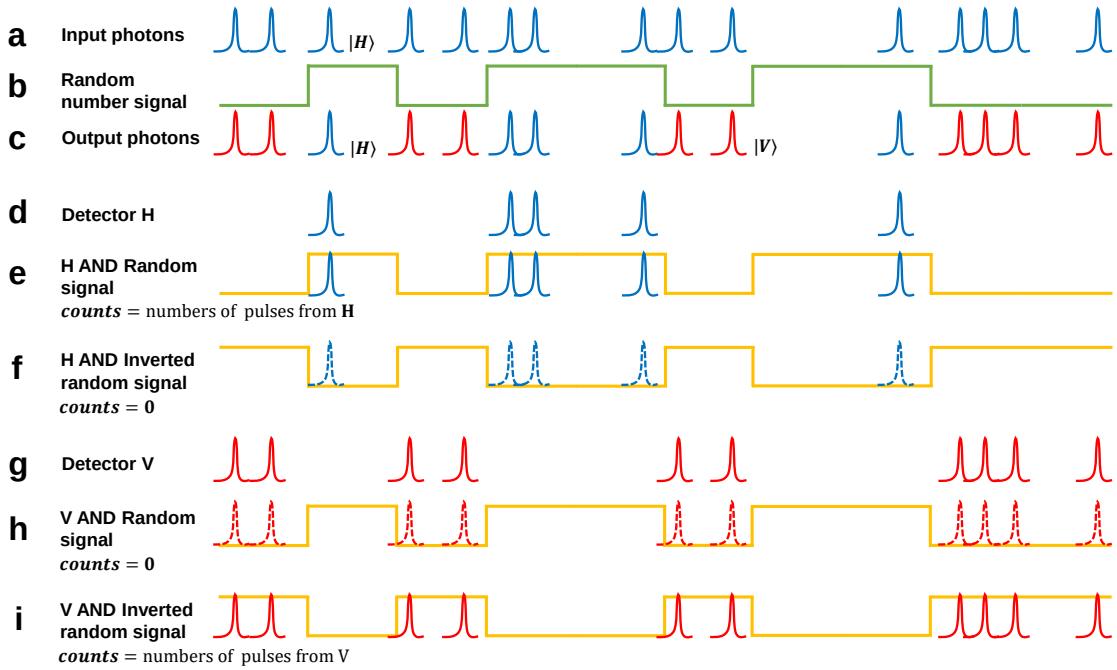

FIG. 4. Schematic diagram of sorting single-photon detection signals with random number signals. (**a**) Horizontally polarized single photons, $|H\rangle$, are sent to EOM. (**b**) Random number signals from QRNG. (**c**) Polarization state of photons coming out from EOM. The polarization states are rotated to $|V\rangle$ (red) if the random bit is "0" and kept to $|H\rangle$ (blue) if the random bit is "1". (**d**) Signals from Detector H. (**e**)/(**f**) The coincidence counts of signals from Detector H and RNS2/inverted RNS2 at the right delay. (**g**) Signals from Detector V. (**h**)/(**i**) The coincidence counts of signals from Detector V and RNS2/inverted RNS2 at the right delay.

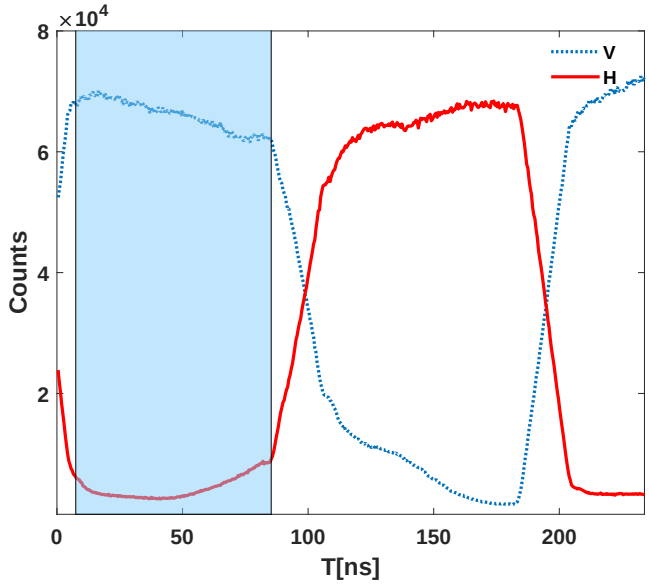

FIG. 5. Measurements of switching contrast with single photons. At the right delay, we send photons in horizontal polarization into EOM and measure the average contrast ratio using 5 MHz driving signal. **H** and **V** represent the photon counts of Detector H, V after the modulation of EOM. We take arithmetic mean of the contrast within the shading area, which is about $C = \frac{Count_V}{Count_H} = 18:1$.

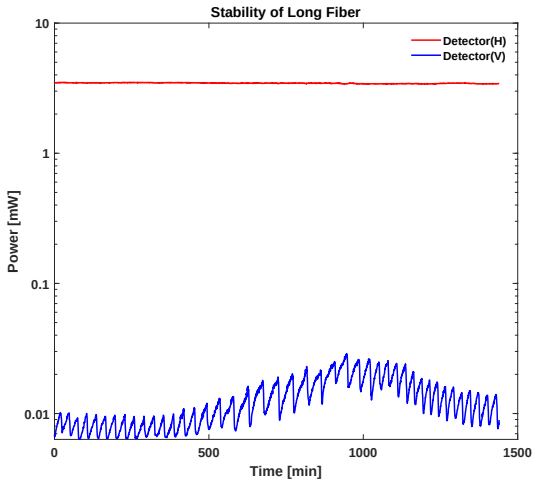

FIG. 6. We send horizontal-like polarized laser light into long fiber in Lab1 and analyze its polarization in Lab2 to monitor the polarization stability of the 215 m fiber across two labs. This measurement lasts for about 24h.

III. CONNECTION: FIBERS AND CABLES

Single-photon detector signals of D1-D4 and D7 in Lab1 are transmitted to Lab2 by five 210 m coaxial cables. The amplitude of pulses from detectors is 4.37V and decreases to 2.84V after passing the long cable while the rising/falling time keeps almost unchanged (6ns/10ns), respectively.

The long fiber used to transmit photon C is 780HP single-mode fiber. It's protected by Polyethylene pipe and a buffer tube. The polarization stability is measured with laser light and shown in Fig.6. Although there are small periodical modulations in power due to the inefficiency of the air conditioner temperature feed-back loop in Lab1, the polarization contrast is maintained to be more than 100 over 24 hours.

IV. ANALYSIS AND EXPERIMENTAL RESULTS

A. Theoretical calculations and experimental data

All the theoretical analyzations are based on the final state $|\psi_{SCA}\rangle$:

$$\begin{aligned}|\psi^f_{SCA}\rangle =&\frac{1}{2}[(\sin\alpha|\mathbf{p}\rangle_S + e^{i\delta}\cos\alpha|\mathbf{w}\rangle_S)|+\rangle_C + (\sin\alpha|\mathbf{p}\rangle_S - e^{i\delta}\cos\alpha|\mathbf{w}\rangle_S)|-\rangle_C]|\alpha\rangle_A\\ &+\frac{1}{2}[(-\cos\alpha|\mathbf{p}\rangle_S + e^{i\delta}\sin\alpha|\mathbf{w}\rangle_S)|+\rangle_C - (\cos\alpha|\mathbf{p}\rangle_S + e^{i\delta}\sin\alpha|\mathbf{w}\rangle_S)|-\rangle_C]|\alpha^\perp\rangle_A, \end{aligned} \quad (6)$$

where we have projected photon A on detection basis $|\alpha\rangle/|\alpha^\perp\rangle$. Particularly, when QRNG gives a bit value of 1, $\alpha = 0$ and $|\psi^f_{SCA}\rangle = \frac{e^{i\delta}}{\sqrt{2}}|\mathbf{w}\rangle_S|V\rangle_C|H\rangle_A - \frac{1}{\sqrt{2}}|\mathbf{p}\rangle_S|H\rangle_C|V\rangle_A$.

Theoretical calculations and experimental results of P_C and P_Q for projecting photon S on $|V\rangle_S$ and $|H\rangle_S$ are shown in Fig.7 and Fig.8, respectively. Note that the data presented in Fig. 7**b** and **d** are identical to that shown in

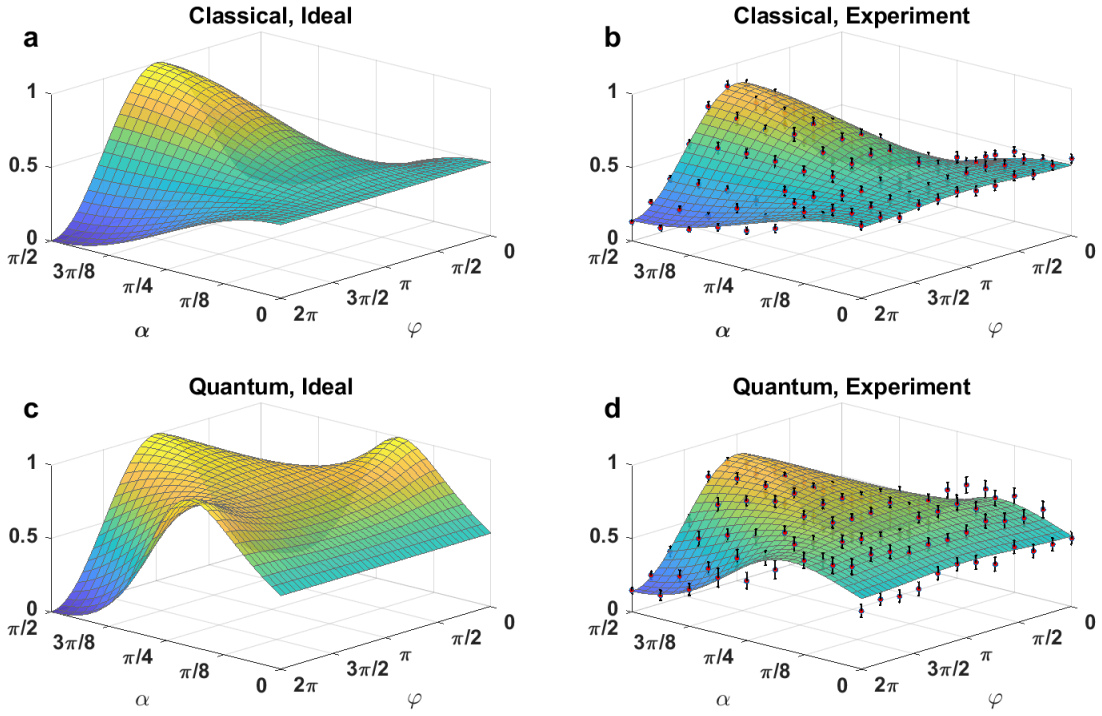

FIG. 7. Demonstration of continuous transitions between particle and wave states in both classical and quantum scenarios. (**a**) Simulated ideal and (**b**) measured probabilities $P_{S=|H\rangle|A=|\alpha^{\perp}\rangle}(\varphi,\alpha)$ for a classical mixture of particle and wave states. We scan the phase φ in MZI for photon S and polarization rotation angle α of photon A. The experimental data are shown in red dots. (**c**) Simulated ideal and (**d**) measured probability $P_{S=|H\rangle|C=|-\rangle,A=|\alpha^{\perp}\rangle}(\varphi,\alpha,\delta)$ for a quantum coherent superposition of particle and wave states. Note that the parameters used to calculate the surface plots for probability distributions shown in (**b**) and (**d**) are based on the values obtained from the independent characterizations of our photon-pair sources, CH gate and polarization contrast. The error bars are derived from Poissonian statistics and error propagations.

the Fig. 3**c** and **f** in the main text. The corresponding equations are:

Fig.7a

$$P_C(|H\rangle_s) = P_{S=|H\rangle|A=|\alpha^{\perp}\rangle}(\varphi,\alpha) = \frac{1}{2}\cos^2\alpha + \sin^2\alpha\sin^2\frac{\varphi}{2} \tag{7}$$

Fig.8a

$$P_C(|V\rangle_s) = P_{S=|V\rangle|A=|\alpha^{\perp}\rangle}(\varphi,\alpha) = \frac{1}{2}\cos^2\alpha + \sin^2\alpha\cos^2\frac{\varphi}{2} \tag{8}$$

Fig.7c

$$P_Q(|H\rangle_s) = P_{S=|H\rangle|C=|-\rangle,A=|\alpha^{\perp}\rangle}(\varphi,\alpha,\delta) = \frac{\frac{1}{2}\cos^2\alpha + \sin^2\alpha\sin^2\frac{\varphi}{2} + \sqrt{2}\cos\alpha\sin\alpha\sin\frac{\varphi}{2}\sin(\delta+\frac{\varphi}{2})}{1+\sqrt{2}\cos\alpha\sin\alpha[\sin\frac{\varphi}{2}\sin(\frac{\varphi}{2}+\delta) - \cos\frac{\varphi}{2}\cos(\frac{\varphi}{2}-\delta)]} \tag{9}$$

Fig.8c

$$P_Q(|V\rangle_s) = P_{S=|V\rangle|C=|-\rangle,A=|\alpha^{\perp}\rangle}(\varphi,\alpha,\delta) = \frac{\frac{1}{2}\cos^2\alpha + \sin^2\alpha\cos^2\frac{\varphi}{2} - \sqrt{2}\cos\alpha\sin\alpha\cos\frac{\varphi}{2}\cos(\frac{\varphi}{2}-\delta)}{1+\sqrt{2}\cos\alpha\sin\alpha[\sin\frac{\varphi}{2}\sin(\frac{\varphi}{2}+\delta) - \cos\frac{\varphi}{2}\cos(\frac{\varphi}{2}-\delta)]}, \tag{10}$$

where φ is the relative phase between the two paths of MZI; α is the angle of projection angle; δ is the phase in ρ_{CA} and equals to 0 in Fig. 7**c**, 8**c**.
$P_{S=|H\rangle|A=|\alpha^{\perp}\rangle}(\varphi,\alpha)$ (P_C in main text) shows a classical mixture of $|\mathbf{w}\rangle$ and $|\mathbf{p}\rangle$;
$P_{S=|H\rangle|C=|-\rangle,A=|\alpha^{\perp}\rangle}(\varphi,\alpha,\delta)$ (P_Q in main text) shows a quantum superposition of $|\mathbf{w}\rangle$ and $|\mathbf{p}\rangle$.
$P_{S=|V\rangle|A=|\alpha^{\perp}\rangle}(\varphi,\alpha) = 1 - P_{S=|H\rangle|A=|\alpha^{\perp}\rangle}(\varphi,\alpha)$;
$P_{S=|V\rangle|C=|-\rangle,A=|\alpha^{\perp}\rangle}(\varphi,\alpha,\delta) = 1 - P_{S=|H\rangle|C=|-\rangle,A=|\alpha^{\perp}\rangle}(\varphi,\alpha,\delta)$.

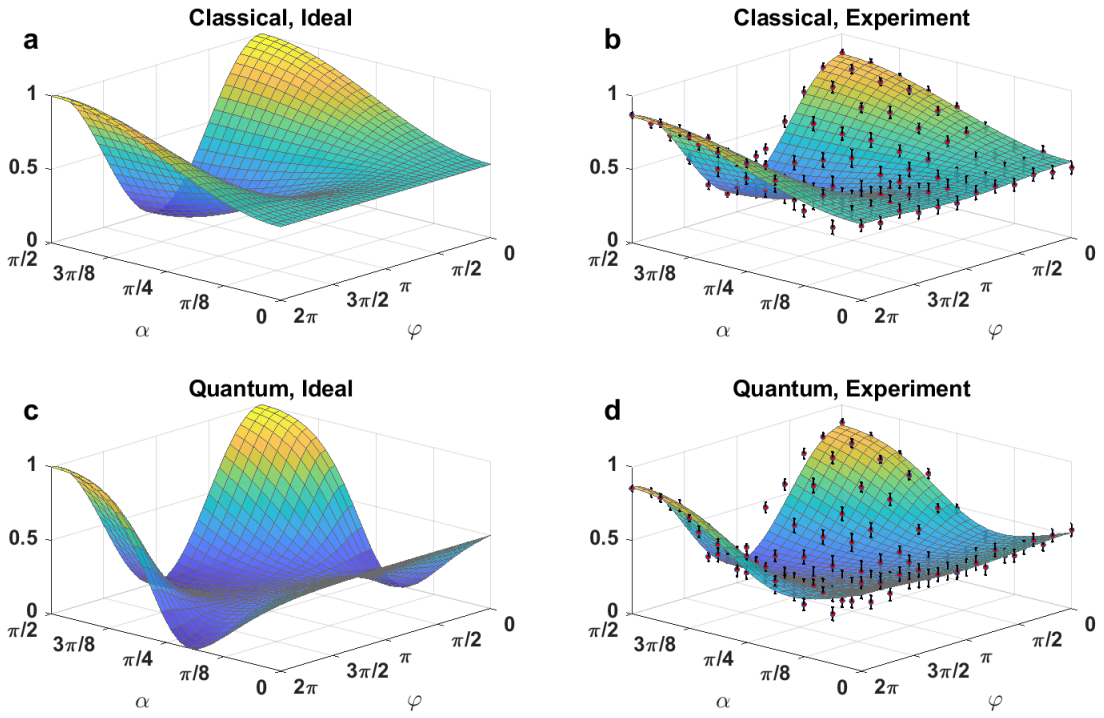

FIG. 8. Complementary results of Fig.7. (**a**) Simulated ideal and (**b**) measured probability $P_{S=|V\rangle|A=|\alpha^\perp\rangle}(\varphi,\alpha)$ for a classical mixture of particle and wave states, where the phase φ in MZI for photon S and polarization rotation angle α of photon A are scanned. The experimental data (red dots) and the theoretical predictions (surface plots) show good agreement. (**c**) Simulated ideal and (**d**) measured probability $P_{S=|V\rangle|C=|-\rangle,A=|\alpha^\perp\rangle}(\varphi,\alpha,\delta)$ for a quantum coherent superposition of particle and wave states. Note that the parameters used to calculate the surface plots for probability distributions shown in (**b**) and (**d**) are based on the values obtained from independent experimental measurements. The error bars are derived from Poissonian statistics and error propagations.

We obtain the above probabilities from the experimental coincidence counts obtained in the experiment:

Fig.7b
$$P_{S=|H\rangle|A=|\alpha^\perp\rangle}(\varphi,\alpha)=\frac{C_{H+\alpha^\perp}+C_{H-\alpha^\perp}}{C_{H+\alpha^\perp}+C_{V+\alpha^\perp}+C_{H-\alpha^\perp}+C_{V-\alpha^\perp}} \tag{11}$$

Fig.8b
$$P_{S=|V\rangle|A=|\alpha^\perp\rangle}(\varphi,\alpha)=\frac{C_{V+\alpha^\perp}+C_{V-\alpha^\perp}}{C_{H+\alpha^\perp}+C_{V+\alpha^\perp}+C_{H-\alpha^\perp}+C_{V-\alpha^\perp}} \tag{12}$$

Fig.7d
$$P_{S=|H\rangle|C=|-\rangle,A=|\alpha^\perp\rangle}(\varphi,\alpha,\delta)=\frac{C_{H-\alpha^\perp}}{C_{H-\alpha^\perp}+C_{V-\alpha^\perp}} \tag{13}$$

Fig.8d
$$P_{S=|V\rangle|C=|-\rangle,A=|\alpha^\perp\rangle}(\varphi,\alpha,\delta)=\frac{C_{V-\alpha^\perp}}{C_{H-\alpha^\perp}+C_{V-\alpha^\perp}}, \tag{14}$$

where C_{ijk} represent the coincidence counts of photons S,C,A with polarization i,j,k conditionally on the detection trigger photon T, respectively. For instance, $C_{H+\alpha^\perp}$ stands for coincidence counts of photons S, C and A with horizontal, diagonally linear and orthogonal to α polarization states.

As mentioned in the main text, the most direct proof for the quantum nature of the wave–particle superposition is to show that the result is sensitive to the relative phase between the wave and particle states, δ. In experiment, we fix $\alpha=\frac{\pi}{4}$ and measure $P_C(|H\rangle_s)$, $P_Q(|H\rangle_s)$, $P_C(|V\rangle_s)$ and $P_Q(|V\rangle_s)$ to show their different dependence on phase δ.

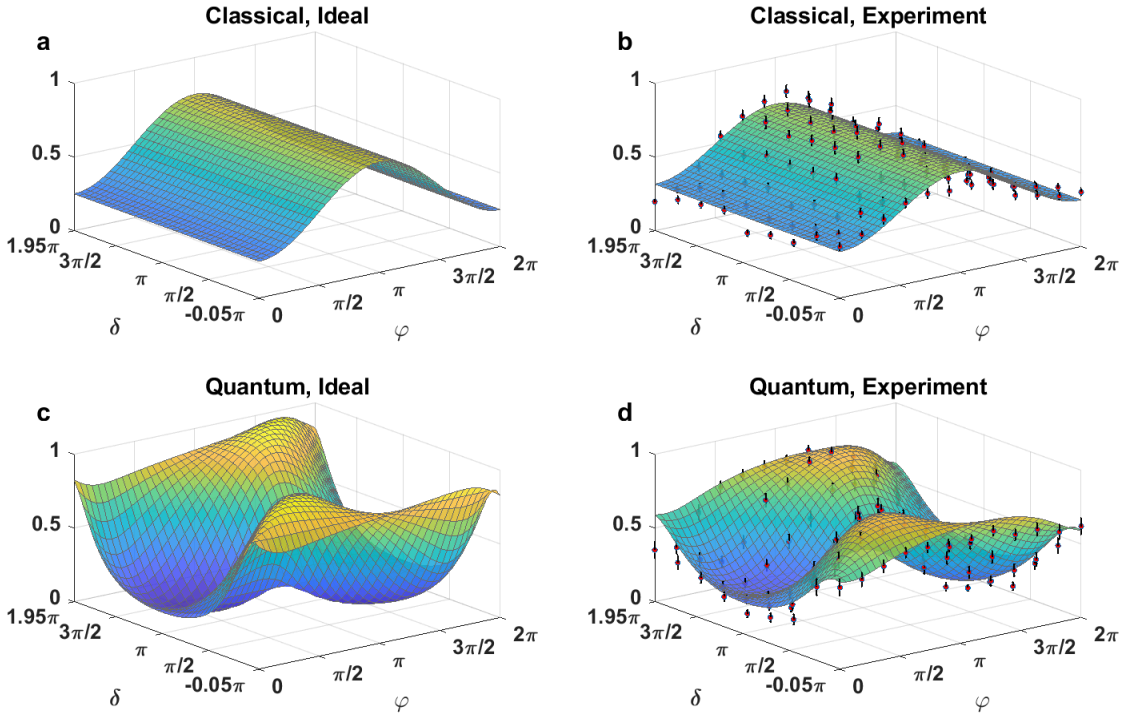

FIG. 9. Witnessing and controlling wave–particle quantum superpositions. We fix $\alpha = \frac{\pi}{4}$ and measure $P_C(|H\rangle_s)$ and $P_Q(|H\rangle_s)$ as functions of the phase φ for photon S and the phase δ between the wave and the particle states of photon S, respectively. (**a**) Simulated ideal and (**b**) measured probability $P_C(|H\rangle_s)$ for a classical mixture of particle and wave states. (**c**) Simulated ideal and (**d**) measured probability $P_Q(|H\rangle_s)$ for a quantum coherent superposition of particle and wave states. $P_C(|H\rangle_s)$ is clearly independent of δ, whereas $P_Q(|H\rangle_s)$ is strongly dependent on δ, manifesting the quantum nature of the superposition of wave and particle states. Note that the parameters used to calculate the surface plots for probability distributions shown in (**b**) and (**d**) are based on the values obtained from independent experimental measurements. The error bars are derived from Poissonian statistics and error propagations.

When $\alpha = \frac{\pi}{4}$, Eq.7-10 give

$$P_C(|H\rangle_s) = P_{S=|H\rangle|A=|\alpha^\perp\rangle}(\varphi) = \frac{1}{4} + \frac{1}{2}\sin^2\frac{\varphi}{2} \tag{15}$$

$$P_C(|V\rangle_s) = P_{S=|V\rangle|A=|\alpha^\perp\rangle}(\varphi) = \frac{1}{4} + \frac{1}{2}\cos^2\frac{\varphi}{2} \tag{16}$$

$$P_Q(|H\rangle_s) = P_{S=|H\rangle|C=|-\rangle,A=|\alpha^\perp\rangle}(\varphi,\delta) = \frac{\frac{1}{4} + \frac{1}{2}\sin^2\frac{\varphi}{2} + \frac{1}{\sqrt{2}}\sin\frac{\varphi}{2}\sin(\delta+\frac{\varphi}{2})}{1 + \frac{1}{\sqrt{2}}[\sin\frac{\varphi}{2}\sin(\frac{\varphi}{2}+\delta) - \cos\frac{\varphi}{2}\cos(\frac{\varphi}{2}-\delta)]} \tag{17}$$

$$P_Q(|V\rangle_s) = P_{S=|V\rangle|C=|-\rangle,A=|\alpha^\perp\rangle}(\varphi,\delta) = \frac{\frac{1}{4} + \frac{1}{2}\cos^2\frac{\varphi}{2} - \frac{1}{\sqrt{2}}\cos\frac{\varphi}{2}\cos(\frac{\varphi}{2}-\delta)}{1 + \frac{1}{\sqrt{2}}[\sin\frac{\varphi}{2}\sin(\frac{\varphi}{2}+\delta) - \cos\frac{\varphi}{2}\cos(\frac{\varphi}{2}-\delta)]} \tag{18}$$

The results are shown in Fig.9-10. Note that the data presented in Fig. 9**b** and **d** are identical to that shown in the Fig. 4**c** and **f** in the main text.

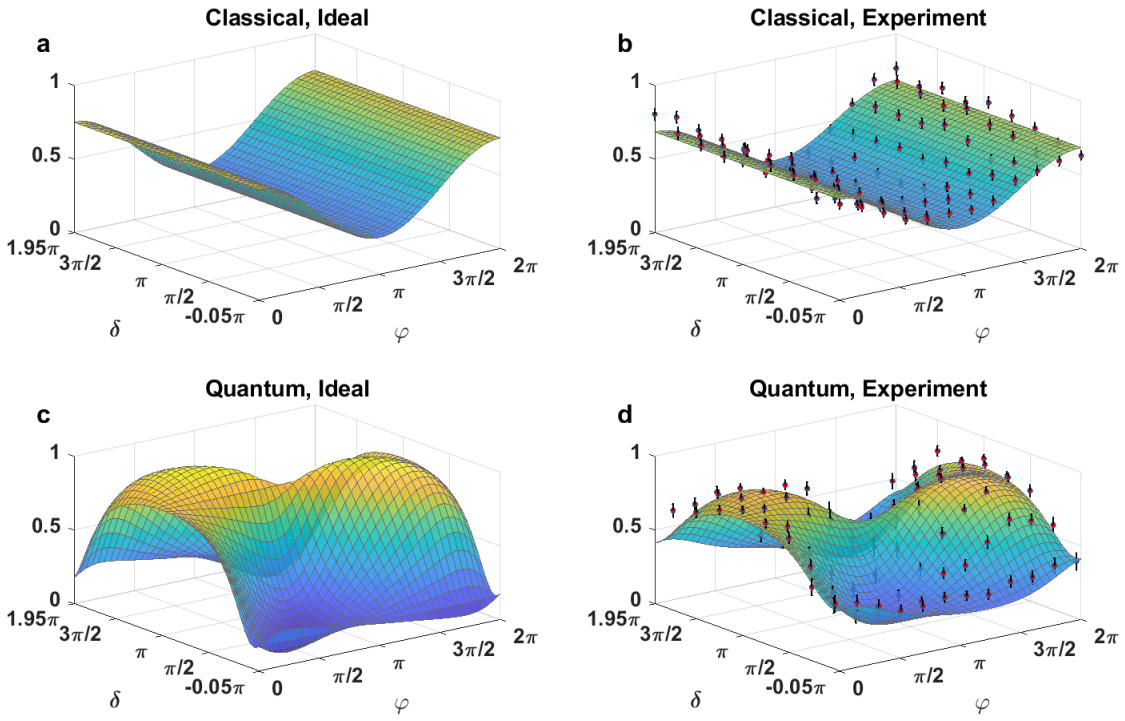

FIG. 10. Complementary results of Fig.9. (**a**) Simulated ideal and (**b**) measured probability $P_C(|V\rangle_s)$ for a classical mixture of particle and wave states. (**c**) Simulated ideal and (**d**) measured probability $P_Q(|V\rangle_s)$ for a quantum coherent superposition of particle and wave states. $P_C(|V\rangle_s)$ is clearly independent of δ, whereas $P_Q(|V\rangle_s)$ is strongly dependent on δ, manifesting the quantum nature of the superposition of wave and particle states. Note that the parameters used to calculate the surface plots for probability distributions shown in (**b**) and (**d**) are based on the values obtained from independent experimental measurements. The error bars are derived from Poissonian statistics and error propagations.

B. Data fitting

One of the main contributions reducing the contrast of our results is the multiphoton emission from SPDC source. Here we introduce parameters to describe the imperfect state. The ideal state of the generated photon pairs are:

$$\rho_{ST} = |VH\rangle\langle VH|_{ST} \tag{19}$$

$$\rho_{CA} = \frac{1}{2}(|HV\rangle + e^{i\delta}|VH\rangle)(\langle HV| + e^{-i\delta}\langle VH|)_{CA}. \tag{20}$$

In our analysis, they are approximated to be Werner states [5]:

$$\rho'_{ST} = F_1\rho_{ST} + \frac{1-F_1}{4}\mathbf{I} \tag{21}$$

$$\rho'_{CA} = F_2\rho_{CA} + \frac{1-F_2}{4}\mathbf{I} \tag{22}$$

with fidelities F_1, F_2, which can be obtained via experimental results. Multiphoton emission reduces both fidelities. Before entering the CZ gate, photon S passes through Hadamard gate ($\mathbf{H_S}$), SBC ($\mathbf{Phi_S}$), W gate ($\mathbf{W_S}$) sequentially. Photon A passes α gate ($\mathbf{Alpha_A}$). We denote all the operations above as $\mathbf{M}_1$ and the current state as ρ_1:

$$\mathbf{M}_1 = \mathbf{W}_S\mathbf{Phi}_S\mathbf{H}_S \otimes \mathbf{Alpha}_A \otimes \mathbf{I}_{CT} \tag{23}$$

$$\rho_1 = \mathbf{M}_1\rho'_{ST} \otimes \rho'_{CA}\mathbf{M}_1^\dagger \tag{24}$$

where

$$\text{Hadmard gate}: \mathbf{H}_{\mathrm{S}} = \begin{bmatrix} \cos\pi/4 & \sin\pi/4 \\ \sin\pi/4 & -\cos\pi/4 \end{bmatrix} \tag{25}$$

$$\text{Phase gate}: \mathbf{Phi}_{\mathrm{S}} = \begin{bmatrix} 1 & 0 \\ 0 & e^{i\varphi} \end{bmatrix} \tag{26}$$

$$\alpha \text{ gate}: \mathbf{Alpha}_{\mathrm{A}} = \begin{bmatrix} \cos\alpha & \sin\alpha \\ \sin\alpha & -\cos\alpha \end{bmatrix}. \tag{27}$$

After the CZ gate, we denote the current state as ρ_2. Multiphoton noise and the imperfect optical components (such as PPBS, wave plates and so on) reduce the interference contrast in Mach-Zehnder interferometer. We approximate the effect as white noise. Under this approximation, the effect contributes to each item of coincidence counts equally. Adding white noise item to ρ_2 gives ρ_2':

$$\rho_2 = \mathbf{CZ}_{SC} \otimes \mathbf{I_{AT}} \rho_1 [\mathbf{CZ}_{SC} \otimes \mathbf{I_{AT}}]^\dagger \tag{28}$$

$$\rho_2' = F_3 \rho_2 + \frac{1 - F_3}{16} \mathbf{I}, \tag{29}$$

where F_3 is related to the HOM interference contrast and hence the fidelity of the CZ gate.

Photon S passes another W gate after CZ gate (Eq. 1) and gives the final state ρ_3:

$$\rho_3 = (\mathbf{W}_S \otimes I_{CAT}) \rho_2' (\mathbf{W}_S \otimes I_{CAT})^\dagger \tag{30}$$

Then we can obtain the following results as functions of the three parameters F_1, F_2 and F_3:

$$\begin{aligned} P_{H+\alpha^\perp} =& \langle H+V|\rho_3|H+V\rangle \\ =& \frac{1}{32}[2F_1F_3(1-\cos\varphi + F_2\cos\varphi\cos 2\alpha) - \sqrt{2}F_2F_3(1+F_1)\sin 2\alpha\cos\delta \\ &+2\sqrt{2}F_1F_2F_3\sin 2\alpha\cos(\delta+\varphi)+2]; \end{aligned} \tag{31}$$

$$\begin{aligned} P_{V+\alpha^\perp} =& \langle V+V|\rho_3|V+V\rangle \\ =& \frac{1}{32}[2F_1F_3(1+\cos\varphi - F_2\cos\varphi\cos 2\alpha) + \sqrt{2}F_2F_3(1+F_1)\sin 2\alpha\cos\delta \\ &+2\sqrt{2}F_1F_2F_3\sin 2\alpha\cos(\delta-\varphi)+2]; \end{aligned} \tag{32}$$

$$\begin{aligned} P_{H-\alpha^\perp} =& \langle H-V|\rho_3|H-V\rangle \\ =& \frac{1}{32}[2F_1F_3(1-\cos\varphi + F_2\cos\varphi\cos 2\alpha) + \sqrt{2}F_2F_3(1+F_1)\sin 2\alpha\cos\delta \\ &-2\sqrt{2}F_1F_2F_3\sin 2\alpha\cos(\delta+\varphi)+2]; \end{aligned} \tag{33}$$

$$\begin{aligned} P_{V-\alpha^\perp} =& \langle V-V|\rho_3|V-V\rangle \\ =& \frac{1}{32}[2F_1F_3(1+\cos\varphi - F_2\cos\varphi\cos 2\alpha) - \sqrt{2}F_2F_3(1+F_1)\sin 2\alpha\cos\delta \\ &-2\sqrt{2}F_1F_2F_3\sin 2\alpha\cos(\delta-\varphi)+2], \end{aligned} \tag{34}$$

where P_{ijk} stands for the probability of obtaining photons S,C,A in i,j,k polarization, conditionally on the detection of photon T. For instance, $P_{H+\alpha^\perp}$ stands for the probability of obtaining photons S,C,A in horizontal, diagonally linear and orthogonal to α polarization states.

Based on the above analysis, we plot the theoretical predictions with the parameters value of $F_1 = 0.98$, $F_2 = 0.90$, $F_3 = 0.61$, as shown in surface plots in Fig.7-10 **b**, **d**.

C. Comparison between the quantum superposition and the classical mixture of wave and particle states in a delayed-choice experiment

To show the difference between quantum superposition and classical mixture of $|\mathbf{w}\rangle$ and $|\mathbf{p}\rangle$, we compared average value and value at $\varphi = 0, \delta = 0$ of them: $P_C = P_{S=|H\rangle|A=|\alpha^\perp\rangle}$ and $P_Q = P_{S=|H\rangle|C=|-\rangle,A=|\alpha^\perp\rangle}$ which are calculated from experimental data. The results are in Fig.11 which shows a clear difference between P_C and P_Q.

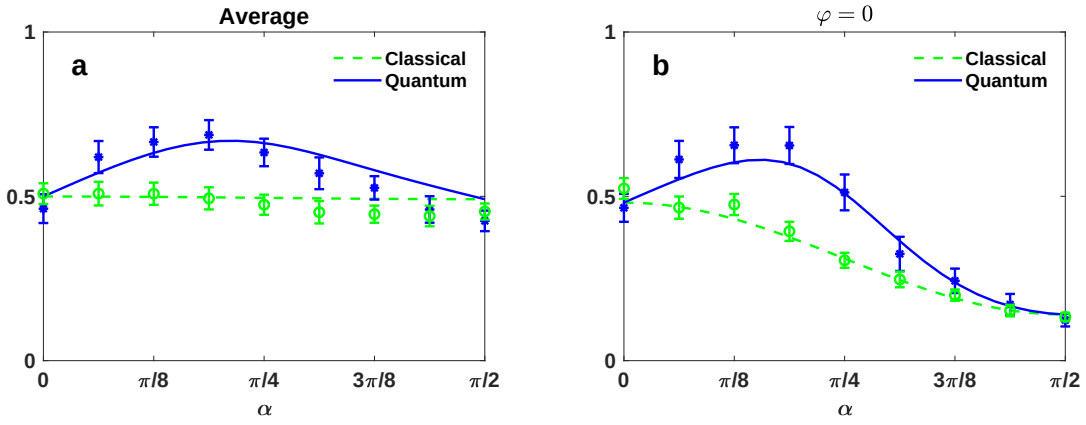

FIG. 11. **(a)** The arithmetic average value of experimental data (P_Q, P_C) under the angle α; **(b)** Value of P_Q, P_C at $\varphi = 0, \delta = 0$. The blue squares and green circles represent our experimental data for P_Q,P_C, respectively. The blue solid and green dash lines are the theoretical predictions.

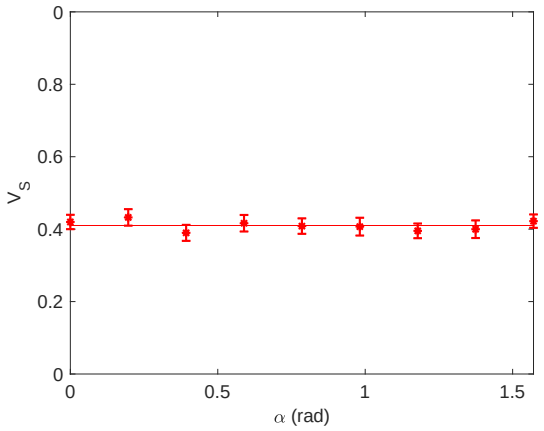

FIG. 12. Visibility obtained from conditional probabilities of photon S without post-selecting on photons C and A by varying α. Red line is the average value of visibilities.

D. Experimental interference visibility of photon S without post-selecting the outcomes of photons C and A

In Ref [6], it has been shown theoretically that one should obtain α-independent interference visibilities if one ignore the outcomes of photons C and A. In our case, it is equivalent to trace out the polarization measurement results of both photons C and A. Ideally, we should obtain $V_s = 0.5$. In Fig.12, we show our result with a nearly constant value 0.41. The discrepancy to the ideal value is mainly due to the limited interference visibility that we obtain experimentally.

[1] C. K. Hong, Z. Y. Ou, and L. Mandel, Phys. Rev. Lett. **59**, 2044 (1987).
[2] N. K. Langford, T. J. Weinhold, R. Prevedel, K. J. Resch, A. Gilchrist, J. L. O'Brien, G. J. Pryde, and A. G. White, Phys. Rev. Lett. **95**, 210504 (2005).
[3] N. Kiesel, C. Schmid, U. Weber, R. Ursin, and H. Weinfurter, Phys. Rev. Lett. **95**, 210505 (2005).
[4] R. Okamoto, H. F. Hofmann, S. Takeuchi, and K. Sasaki, Phys. Rev. Lett. **95**, 210506 (2005).
[5] R. F. Werner, Phys. Rev. A **40**, 4277 (1989).
[6] R. Ionicioiu, T. Jennewein, R. B. Mann & D. R. Terno *Nat. Commun.* **5**, 3997 (2014).